

Optical Engineering

OpticalEngineering.SPIEDigitalLibrary.org

Passively aligned multichannel fiber-pigtailing of planar integrated optical waveguides

Johannes Kremmel
Tobias Lamprecht
Nino Crameri
Markus Michler

SPIE.

Johannes Kremmel, Tobias Lamprecht, Nino Crameri, Markus Michler, "Passively aligned multichannel fiber-pigtailing of planar integrated optical waveguides," *Opt. Eng.* **56**(2), 026115 (2017), doi: 10.1117/1.OE.56.2.026115.

Passively aligned multichannel fiber-pigtailing of planar integrated optical waveguides

Johannes Kremmel,^{a,*} Tobias Lamprecht,^b Nino Crameri,^b and Markus Michler^a

^aInterstate University of Applied Sciences Buchs NTB, Buchs, St. Gallen, Switzerland

^bVario-optics AG, Heiden, Appenzell Ausserrhoden, Switzerland

Abstract. A silicon device to simplify the coupling of multiple single-mode fibers to embedded single-mode waveguides has been developed. The silicon device features alignment structures that enable a passive alignment of fibers to integrated waveguides. For passive alignment, precisely machined V-grooves on a silicon device are used and the planar lightwave circuit board features high-precision structures acting as a mechanical stop. The approach has been tested for up to eight fiber-to-waveguide connections. The alignment approach, the design, and the fabrication of the silicon device as well as the assembly process are presented. The characterization of the fiber-to-waveguide link reveals total coupling losses of (0.45 ± 0.20) dB per coupling interface, which is significantly lower than the values reported in earlier works. Subsequent climate tests reveal that the coupling losses remain stable during thermal cycling but increases significantly during an 85°C/85 Rh-test. All applied fabrication and bonding steps have been performed using standard MOEMS fabrication and packaging processes. © The Authors. Published by SPIE under a Creative Commons Attribution 3.0 Unported License. Distribution or reproduction of this work in whole or in part requires full attribution of the original publication, including its DOI. [DOI: [10.1117/1.OE.56.2.026115](https://doi.org/10.1117/1.OE.56.2.026115)]

Keywords: integrated optics; waveguides; single-mode fibers; arrays; passive alignment.

Paper 161646 received Oct. 21, 2016; accepted for publication Feb. 2, 2017; published online Feb. 16, 2017.

1 Introduction

A large number of active and passive optical components (e.g., beam-splitters and multiplexers) can be realized using integrated waveguides or planar lightwave circuits (PLCs) in a very compact fashion. As fibers are used to create communication links over long distances and to connect laser- and photo-diodes to such PLCs, the reliable coupling of fibers to waveguides is highly important.

In recent years, various methods have been reported for fiber-to-waveguide coupling. There are single-channel connections where fibers are aligned actively and attached by adhesive bonding. Other approaches include the application of out-of-plane couplers to couple into a fiber.¹ For multimode systems, various passive alignment methods have been presented. For example, waveguide structures are used as an aligning element centering a fiber in front of a waveguide core.² Furthermore, multifiber connections have been reported with an mechanical transfer-connector inspired approach, using guiding pins to realize passive alignment.^{3,4} For multifiber single-mode coupling, mainly fiber arrays in a glass substrate are actively aligned to the PLC and attached by adhesive bonding. Kraehenbuehl et al.⁵ presented a method for single-channel coupling, based on silicon V-grooves and integrated alignment structures on the waveguide board to realize a passive alignment of single-mode waveguides and fibers. Their approach integrates a ferrule to attach a connector directly to the waveguide board. A major disadvantage of this approach is the extensive space requirement for the connector, which spoils the high integration density of PLCs. In Ref. 6, the coupling of multiple fibers to polymer waveguides is presented. By using one single mask to structure

the waveguide cores and silicon waveguides, a high accuracy of the alignment has been achieved, but a very specific process had to be applied. In Ref. 7, this approach has been adapted to couple fibers to integrated silica waveguides.

2 Alignment Approach

The main goal of this work is an easy multifiber pigtailling of PLC boards without additional active alignment tools. To achieve a passive alignment, eight fibers are mounted onto a silicon device equipped with eight V-grooves for the fibers and additional V-grooves as an alignment feature, as shown in Fig. 1. To actually couple the fibers to the waveguides, the assembled fiber array is bonded onto a PLC board based on polymer waveguides, similar to the ones shown in Refs. 5 and 8, with a coupling interface consisting of eight waveguides and alignment features corresponding to the V-grooves on the silicon device. During the assembly, the silicon device is aligned by waveguide structures (see Fig. 2), and the fibers are positioned accurately in front of the waveguide. Thus, a compact device, featuring a fiber pitch of 250 μm , can be realized.

2.1 Alignment Concept

The alignment device consists of eight V-grooves to mount the eight fibers and three V-grooves for the alignment. The width of all V-grooves was chosen to be the same. Essentially, the device could be small (<10 mm²), but for ease of handling we chose the size of the device to be 10 mm \times 5 mm. On the corresponding waveguide board, depicted in Fig. 1(b), there are three alignment structures and eight waveguides arranged matching to the V-grooves on the silicon device.

When the silicon device, which holds the fibers, and the waveguide board are assembled together, the silicon surface

*Address all correspondence to: Johannes Kremmel, E-mail: johannes.kremmel@ntb.ch

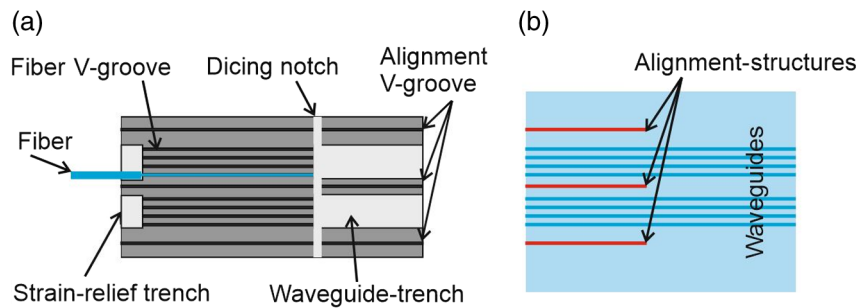


Fig. 1 Schematic design of (a) the silicon device and the (b) PLC coupling interface on the waveguide board.

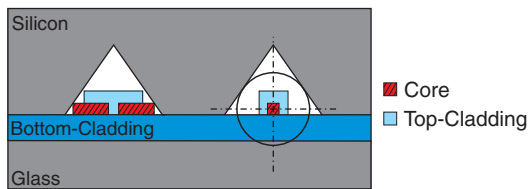


Fig. 2 Cross section of a V-groove with alignment structure (left) and position of a fiber in front of the waveguide (right).

is in contact with the bottom cladding of the waveguide board. This provides accurate vertical alignment. By choosing the right width of the V-groove, the height of the fiber in front of the waveguide can be adjusted. For optimal coupling, the center of the fiber has to be matched to the center of the waveguide (compare Fig. 2).

The lateral position of the fiber is adjusted by alignment structures, which define the position of the alignment grooves. To achieve maximum position precision and accuracy, the alignment structures are fabricated in the same processing step as the waveguide cores. A top-cladding structure was added to enable precentering during assembly (see left side of Fig. 2).

In the axial position, the distance between the fiber facet and the waveguide facet has to be minimized to achieve maximum coupling efficiency. The fiber facets and the waveguide facets act as a mechanical stop. By pushing the silicon device and the board against each other, a minimal gap between the fiber and waveguide facets can be achieved.

2.2 Simulation of the Fiber-Coupling Characteristics

To determine the necessary position accuracy, the coupling characteristics of a 9/125 μm single-mode fiber (e.g., SMF-28) to an integrated polymer waveguide have been investigated using beam propagation method simulations. The integrated waveguides exhibit a refractive index difference $\Delta n = 0.006$, a width of 5 μm , and a height of 5 μm . The simulations reveal that a transition loss of 0.18 dB has to be expected due to the mismatch of the modal fields of fiber and waveguide.

Assuming a displacement loss of up to 0.5 dB as acceptable, a placement error of up to 1.5 μm can be tolerated, according to Fig. 3. The investigation of angular errors revealed that a tilt angle of up to 1.2 deg can be tolerated. Because there is a large overlap between the PLC board and the silicon device, the tilt errors are expected to be small. Considering an overlap length of 4 mm, a tilt angle

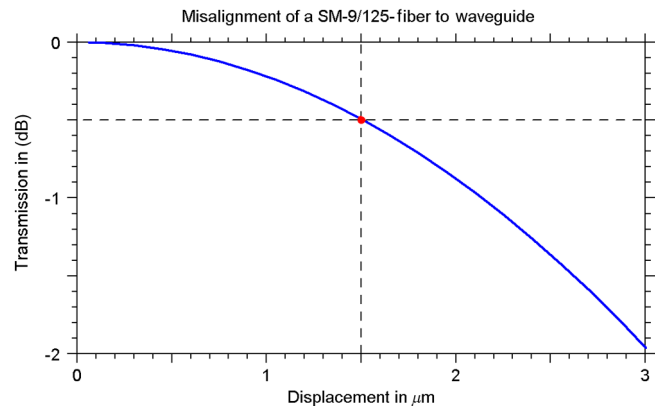


Fig. 3 Displacement dependency of the fiber-to-waveguide coupling efficiency.

of 1 deg would result in an offset of 70 μm . This is large compared to the necessary position accuracy of 1.5 μm . Thus, tilt errors can be neglected.

3 Design and Fabrication of the Components

Based on the alignment concept, the individual components had to be designed and fabricated.

3.1 Design and Fabrication of the Silicon Device

To fabricate the silicon device, we used standard MEMS fabrication processes based on photolithography and potassium hydroxide (KOH) etching. The V-grooves were formed by {111} surfaces, allowing the precise fabrication of V-grooves with a desired width.⁹ Assuming a waveguide height H of 5 μm and a fiber diameter F of 125 μm , the center of the fiber has to be positioned 2.5 μm above the bottom cladding level (see Fig. 4). Considering the angles of the {111}-type surfaces, a V-groove width V of 156.7 μm results. To obtain V-grooves with an accurate width, all etching processes have to be tightly controlled to avoid over etching. In preceding tests, the occurring undercut, which widens the V-grooves, has been measured and subsequently compensated for on the photomask.

3.2 Mounting of the Fibers onto the Silicon Device

To finalize the silicon device, the fibers (Corning SMF-28e+) have to be mounted into the respective V-grooves (see Fig. 5). For low-loss coupling of multiple fibers, all fiber facets have

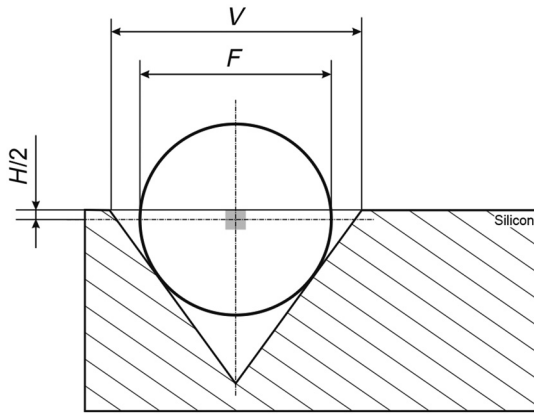


Fig. 4 Cross section of the coupling system consisting of the silicon V-groove and the fiber; the waveguide is indicated as a gray square.

to be aligned coplanar. One way to achieve this is to cleave the fibers and mount the fibers with an accurate z -position onto the silicon device. A disadvantage of this approach is that the position of each fiber has to be adjusted individually. Additionally, a very precise amount of adhesive has to be applied to bond the fibers to the silicon device without voids while avoiding wetting of the fiber facets. To avoid these issues, we chose to adjust the lengths of the fibers after the adhesive bonding using a wafer dicer. By cutting a notch [see Fig. 1(a)], the resulting fiber facets are arranged in one single line and protruding adhesive is removed. The resulting fiber facets provide the mechanical stop for the facet of the waveguide board; therefore, the actual position of the notch does not need to be very accurate as long as it is perpendicular to the V-grooves.

While one fiber after another was fed into the V-grooves, a UV transparent glass lid was used to clamp the fibers down into the grooves. To attach the fibers to the silicon device, a UV curable adhesive was applied into the strain-relief trench. By capillary forces, the adhesive was drawn into the fiber equipped V-grooves, effectively filling up the gaps between the fibers and the silicon device. After the curing step with UV-light, the fibers were cut to length. Thus, all eight fiber facets were precisely arranged in one line and excess adhesive was removed. The applied cutting process produced fiber facets with an RMS roughness of 75 to 100 nm.

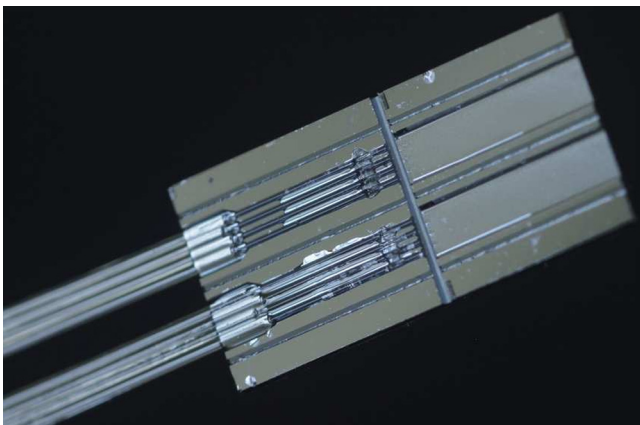


Fig. 5 Photography of the silicon device equipped with eight fibers.

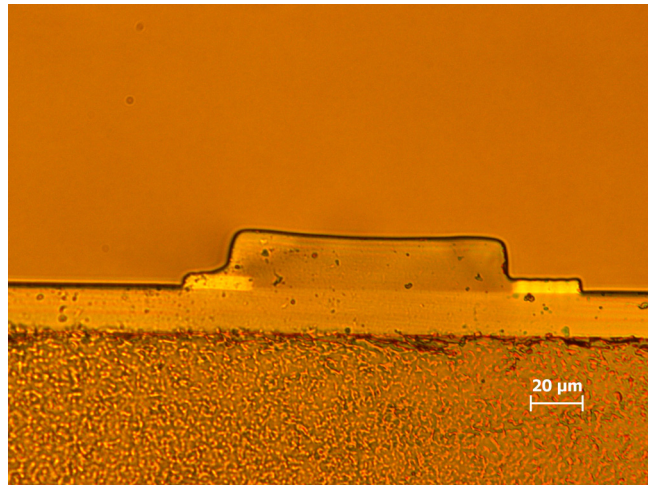


Fig. 6 Bottom illuminated microscopy picture of a cross section of an alignment structure.

3.3 Fabrication of the Waveguide Board

The waveguides used in our device were fabricated similar to Ref. 8. As a first step, a bottom cladding layer was deposited onto a glass substrate and cured by a UV flood exposure. As a second step, a layer of core material was applied. To structure the core layer, the material was cured using a laser direct imaging machine followed by removing the uncured material by a development step. Subsequently, a layer of cladding material was applied as top cladding. Using the laser direct writing setup equipped with a second laser, featuring a beam diameter of $45 \mu\text{m}$, and a subsequent developer rinse, all waveguides were covered with a line of cladding material. Additionally, a support structure was added to the alignment structures (see Fig. 6).

3.4 Assembly of the Coupling System

To achieve optical coupling between the fibers on the silicon device and the integrated waveguides, the two parts have to be joined. When the joining is done manually, there is a tactile feedback when the silicon device snaps correctly into place. Additionally, interference fringes can be observed when viewing through the glass substrate. This confirms close proximity between the silicon device and lower cladding. To attach the silicon device to the PLC board, the two parts were pressed together and UV curable adhesive, which allows a quick bonding, was applied. Additionally, the adhesive acts as index-matching agent in the gap between waveguide and fiber facet. In Fig. 7, a photograph of an assembled system is shown.

4 Measurement and Results

Following the fabrication and assembly of the system, the coupling characteristics as well as the positioning accuracy were investigated. Finally, two different tests in a climate chamber were performed to investigate the reliability and aging behavior of the assembly.

4.1 Microscopy Analysis of the Assembled System

In the first step, a microscopy analysis was done to characterize the joining process and the passive alignment of the two devices. The microscopy analysis on cross sections using

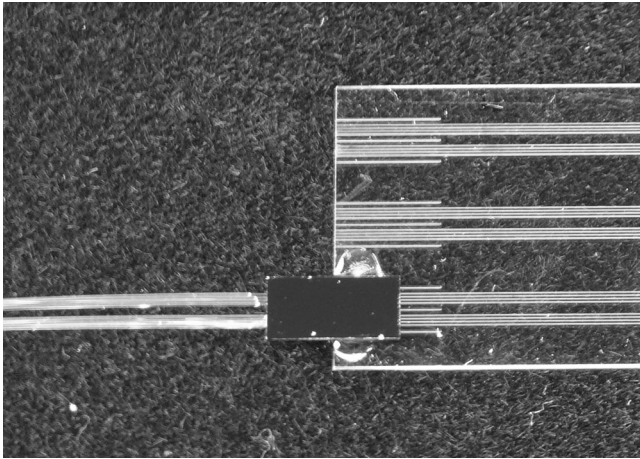


Fig. 7 Assembled connection of eight fibers to eight waveguides.

bottom illumination confirmed the proper alignment of the silicon device and the waveguide (see Fig. 8).

The lateral deviation of the silicon device to the alignment structures is in the range of about $1 \mu\text{m}$ or less. One can also observe that the device is closely attached to the waveguide board without a gap between the bottom cladding and the devices surface (Fig. 8). Figure 9 shows that the fiber fits tightly to the V-groove and therefore has the desired linear support.

Microscopy analysis also allowed the measurement of the waveguide geometry and the width of the V-groove. The waveguides have a height of $5 \mu\text{m}$ and a width of $5 \mu\text{m}$. The V-grooves are about $157 \mu\text{m}$ wide.

4.2 Characterization of the Optical Path

The coupling losses caused by the passively coupled interface have been identified. For this reason, we compared measurements on actively aligned reference waveguides and passively aligned waveguides. To couple light into the waveguides, an SMF-28e+ fiber connected to a 1310-nm diode laser was used as the light source. The stability of the output power was monitored using a fiber beam splitter.

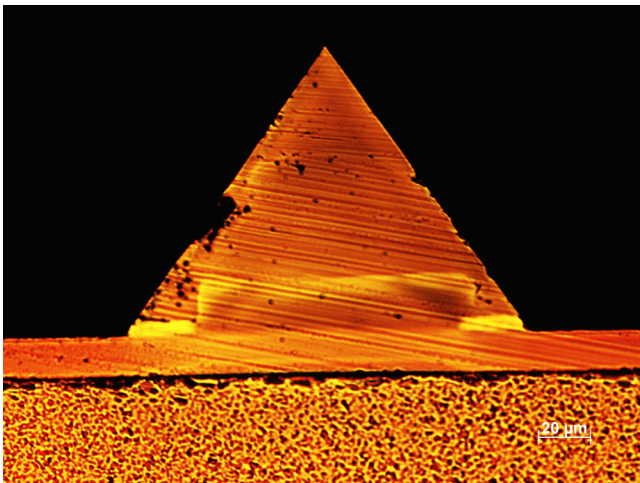


Fig. 8 Cross section of an alignment structure fitting into a V-groove.

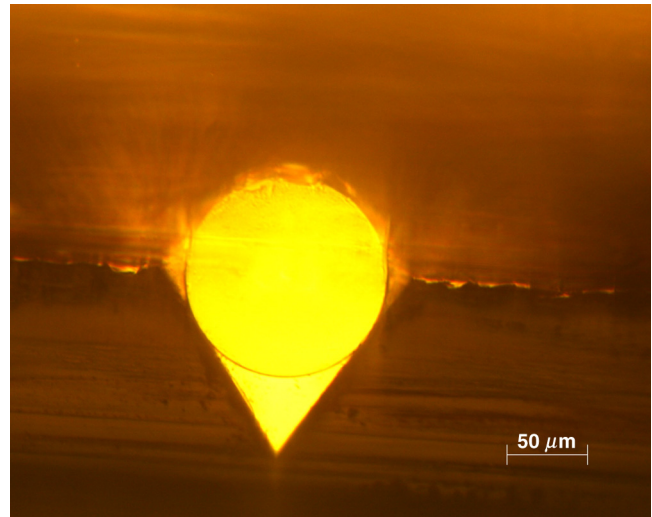


Fig. 9 Cross section of a silicon device with mounted fiber.

During the reference measurements, the output power of the polymer waveguide has to be measured to determine the transmission properties of the waveguides. A multimode fiber with a core diameter of $105 \mu\text{m}$ and an NA of 0.2 coupled to a Newport 818-IS integrating sphere was used as a detector [compare Fig. 10(a)]. To compensate for fiber and coupling losses in the setup, a calibration measurement was performed by measuring the input power of the feeding fiber directly with the multimode detector fiber [Fig. 10(b)].

In the second step, the passively aligned optical link was measured. During these measurements, the light source remained the same as during the reference measurements. On the output side, the passively coupled SMF-28e+ fibers were connected directly to the integrating sphere [see Fig. 10(c)]. Again, a calibration measurement was performed by measuring the waveguide input power by connecting the input fiber directly to the integrating sphere [Fig. 10(d)]. During all measurements, the gaps have been filled with index-matching gel.

The results obtained by the reference measurements (see Table 1) show that the waveguides, with a length of 25 mm, exhibit average transmissions of -1.69 dB . When the fiber

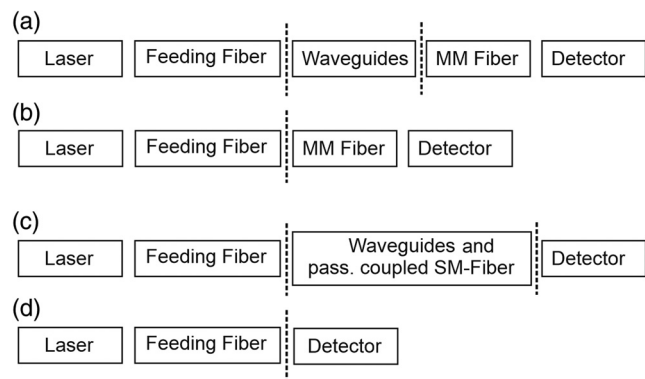


Fig. 10 Block diagram of the measurement procedure for characterization of the optical link: (a) measurement: reference, (b) calibration: reference, (c) measurement: ribbon, and (d) calibration: ribbon.

Table 1 Measurement data of the optical characterization (transmission and coupling loss), including average and standard deviation σ .

Channel	$T_{\text{Reference}}$ (dB)	$CL_{\text{Reference}}$ (dB)	T_{Ribbon} (dB)	CL_{Ribbon} (dB)
A	-2.00	0.93	-1.86	0.78
B	-1.99	0.92	-1.86	0.79
C	-1.65	0.58	-1.84	0.76
D	-1.63	0.55	-2.07	1.00
E	-1.61	0.53	-1.95	0.88
F	-1.55	0.47	-1.88	0.81
G	-1.46	0.38	-2.04	0.97
H	-1.68	0.60	-1.89	0.81
Average	-1.69	0.62	-1.92	0.85
σ	0.19	0.19	0.08	0.08

Table 2 Results of the aging and thermal cycling of the sample.

Measurement	T_{Ribbon} (dB)	σ (dB)
Initial	1.92	0.08
14 days	1.86	0.13
T-cycling	1.89	0.15
85/85-test	3.13	1.20

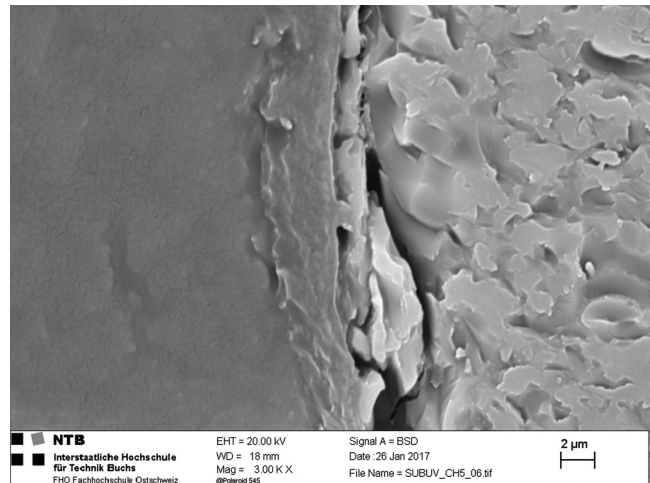
ribbon is attached to the waveguides, they exhibit transmissions of about -1.92 dB. Previous cut-back measurements show that the polymer waveguides exhibit a propagation loss of 0.43 dB/cm. Considering the length of the polymer waveguide sample of 25 mm, a propagation loss of 1.08 dB has to be expected. Thus, coupling losses $CL_{\text{Reference}}$ for the reference waveguides and CL_{Ribbon} for the fiber coupled waveguides can be calculated. Neglecting scattering losses due to surface irregularities, one can assume a lossless coupling between a single-mode waveguide and a multimode fiber during the reference measurement. Thus, a coupling loss of 0.23 dB between single-mode waveguide and single-mode fiber can be determined by subtracting $CL_{\text{Reference}}$ from CL_{Ribbon} .

4.3 Climate Tests

After the initial measurements, the sample was stored at room temperature for 14 days, followed by a second transmission measurement, which was performed as reference measurement for thermal cycling. In the cycling test, our sample was heated to 70°C and cooled to -30°C 10 times with a dwell time of 15 min each. The slope of the temperature ramp was ± 1 K, while the humidity was free-floating. After the thermal cycling, a third transmission measurement was performed. Subsequently, the sample was exposed to an 85/85-test. In this testing scheme, the sample was exposed

Table 3 Summarized measurement data.

$CL_{\text{Reference}}$	0.62 dB	Total coupling loss, reference
CL_{Ribbon}	0.85 dB	Total coupling loss, ribbon
ΔCL	0.23 dB	Excess loss by passive SMF-coupling
$CL_{\text{Mode-Mismatch}}$	0.18 dB	Simulated loss by mode mismatch
$CL_{\text{Position-Error}}$	0.05 dB	$\Delta CL - CL_{\text{Mode-Mismatch}}$
Scatter loss (SL_{tot})	0.44 dB	$CL_{\text{Ribbon}} - CL_{\text{Mode-Mismatch}} - \Delta CL$
$SL_{\text{interface}}$	0.22 dB	Per interface
$CL_{\text{WG-SMF}}$	(0.45 ± 0.20) dB	Total coupling loss per fiber-waveguide interface

**Fig. 11** SEM image of the damaged coupling interface. The waveguide on the right side is in contact with the adhesive, which delaminated from the fiber on the left side.

to 85°C with a relative humidity of 85% for 168 h. After finishing the test, a final transmission measurement was performed.

Table 2 shows that the transmission values remained almost unchanged during the storage period and the thermal cycling. During the 85/85-test, the transmission decreased to -3.13 dB on average. As the standard deviation of 1.2 dB after the 85/85-test indicates, the variance of the measured values increased significantly after the 85/85-test. While two of the channels remained almost unchanged at -1.9 and -2.1 dB after the 85/85-test, the other channels exhibited transmissions of down to -5.50 dB.

5 Conclusions

The passive alignment of eight waveguides in one single step was demonstrated with coupling losses of about 0.23 dB. This is very close to the simulated losses due to mode mismatch of 0.18 dB, indicating a very accurate positioning of the fibers. Referring to Fig. 3, the positioning error is about 0.5 μm . The summarized results in Table 3 show that

there are excess losses of 0.22 dB per waveguide to fiber transition ($SL_{\text{interface}}$). These excess losses are caused by surface irregularities on the waveguide and fiber facets. We assume that these defects are equally distributed on the facets and are the main reason for the variance of the measured values. Thus, we expect that each interface causes 50% of these losses. By calculating the combined standard deviation according to the propagation of uncertainty, we estimate a margin of ± 0.20 dB. The total coupling losses can be calculated as $CL_{\text{WG-SMF}} = CL_{\text{Position-Error}} + CL_{\text{Mode-Mismatch}} + SL_{\text{interface}}$. Considering these assumptions, we estimate that the total coupling losses $CL_{\text{WG-SMF}}$ are 0.45 ± 0.20 dB for each passively coupled waveguide to single-mode fiber interface. The measured coupling losses are significantly lower than the results reported in Refs. 5 and 6, which have been 0.8 and 0.7 dB, respectively. Remarkably, these reported values represent only the losses imposed by position error.

The results of the climate tests reveal that the coupling losses remain unchanged after thermal cycling. After the subsequent 85/85-test, the measured transmission values show a large variance. There are two channels with unchanged performance. Thus, we conclude that the performance of the waveguides remained stable during the test. A microscopy analysis revealed that there are no handling defects on exposed optical surfaces. Scanning electron microscope (SEM) analysis of cross sections of the assembly revealed that delamination of the adhesive at the fibers front surface on the channels occurred, which increased losses values (see Fig. 11). On channels with unchanged loss values, the interface on both sides of the gap remained intact. An optimization of the attachment process (e.g., plasma activation) could increase the adhesion of the adhesive to the front surface of the fiber to achieve a more robust assembly.

The presented coupling method provides a passive alignment based on mechanical stops and mechanical alignment structures. This means the assembly can be done manually with tweezers without any additional alignment tools. A further advantage is that the fabrication of the silicon device and the wafer mounting are done using standard MOEMS fabrication and packaging processes, such as anisotropic silicon etching in KOH, adhesive bonding, and wafer dicing, avoiding any polishing process.

Acknowledgments

The research was funded by the Commission for Technology and Innovation in Switzerland under Contract No. 16259.2 PFEN-NM.

References

1. D. Taillaert et al., "An out-of-plane grating coupler for efficient butt-coupling between compact planar waveguides and single-mode fibers," *IEEE J. Quantum Electron.* **38**, 949–955 (2002).
2. M. McFarland and K. Beeson, "Polymer microstructures which facilitate fiber optic to waveguide coupling," U.S. Patent No. 5,359,687 (1994).
3. D. Jubin et al., "Polymer waveguide-based multilayer optical connector," *Proc. SPIE* **7607**, 76070K (2010).
4. T. Bierhoff et al., "All optical pluggable board-backplane interconnection system based on an MPX™-FlexTail connector solution," in *Photonics Society Winter Topicals Meeting Series (WTM), 2010 IEEE*, pp. 91–92 (2010).
5. R. Kraehenbuehl et al., "High-precision, self-aligned, optical fiber connectivity solution for single-mode waveguides embedded in optical PCBs," *J. Lightwave Technol.* **33**, 865–871 (2015).
6. R. Moosburger et al., "Passive alignment of single-mode fibers to integrated polymer waveguide structures utilizing a single-mask process," *IEEE Photonics Technol. Lett.* **11**, 848–850 (1999).
7. R. Hauffe et al., "Methods for passive fiber chip coupling of integrated optical devices," in *2000 Proc. of the 50th Electronic Components and Technology Conf.*, pp. 238–243 (2000).
8. E. Zraggen et al., "Laser direct writing of single-mode polysiloxane optical waveguides and devices," *J. Lightwave Technol.* **32**, 3036–3042 (2014).
9. K. Sato et al., "Tenth IEEE international workshop on micro electro mechanical systems characterization of orientation-dependent etching properties of single-crystal silicon: effects of KOH concentration," *Sens. Actuators A Phys.* **64**(1), 87–93 (1998).

Johannes Kremmel received his engineer diploma in systems engineering from the University of Applied Sciences Buchs NTB, Switzerland, in 2005. In 2010, he received his master's degree in optical systems technology from the University of Applied Sciences Ravensburg-Weingarten, Germany. Since 2006, he has worked at the Institute for Micro- and Nanotechnology of the NTB. His current research interests include optical interconnects, optical simulations, and packaging of optical systems.

Tobias Lamprecht received his PhD from the University of Twente, Enschede, The Netherlands, in 2011 and graduated in systems engineering, integrated microsystems, and optical systems from the University of Applied Sciences NTB Buchs, in 2000, 2003, and 2007, respectively. He is the chief technology officer of Vario-optics AG, developing polymer waveguide-based electro-optical circuit boards. Between 2004 and 2010, he worked as an engineer for IBM Research Zurich, Switzerland, pursuing research on polymer optical waveguides.

Nino Cramer received his bachelor's degree in systems engineering with a focus on integrated microsystems from the University of Applied Sciences NTB Buchs in 2010 and his master of science in engineering with a focus on industrial technologies from the University of Applied Sciences of Eastern Switzerland in 2012. He works as a process engineer at Vario-optics AG, developing and establishing processes for the fabrication of polymer optical waveguide systems.

Markus Michler received his PhD from the University of Vienna in 2001 after completing his diploma work in quantum optics from the University of Innsbruck. He is a lecturer for micro- and nanotechnology, photonics, and physics at the University of Applied Sciences of Technology Buchs, NTB. He is mainly working on projects in the field of optical packaging, MOEMS, fiber optics, and planar integrated optics.